DEVELOPMENT OF A JOINT REGIONAL BODY AND SURFACE WAVE TOMOGRAPHY METHOD

William L. Rodi[1] and Delaine T. Reiter[2]

Massachusetts Institute of Technology[1]
Weston Geophysical Corporation[2]

Sponsored by Air Force Research Laboratory

Contract No. FA8718-04-C-0027

ABSTRACT

Inadequately modeled Earth structures cause systematic biases in predictions of geophysical parameters such as the travel times and amplitudes of regional seismic phases. More accurate and reliable predictions of these quantities (especially in aseismic regions) are needed to improve nuclear monitoring efforts to detect, locate and discriminate regional events.

To specifically help improve regional location capabilities, Weston Geophysical Corporation and the Massachusetts Institute of Technology are collaborating on the development of a joint body-wave/surface-wave inversion method to derive self-consistent 3-D *P* and *S* velocity models for the crust and upper mantle. The method expands on our current *Pn* travel-time tomography algorithm, which uses finite-difference ray tracing to model body-wave travel times in 3-D Earth models. Surface-wave group delays (group travel times) are modeled in a two-step procedure. The first step calculates phase- and group-velocity dispersion curves at each point of a latitude/longitude grid, applying 1-D dispersion modeling to the velocity-depth profile for each point. The second step employs 2-D finite-difference ray tracing to the resulting phase-velocity maps, period by period, and then integrates the group-velocity maps along the derived ray paths to obtain group delays. The use of 2-D ray tracing accounts approximately for the non-great circle propagation of surface waves in 3-D Earth structures. Our inversion approach will follow these steps in reverse. Group-velocity maps will be fit to observed group delays along particular source-receiver paths, and the resulting group-velocity dispersion curve for each geographic grid point will be used to determine an updated velocity-depth profile for the point, using a 1-D inversion technique. Our approach uses the first-arrival body-wave travel times to directly update the 3-D *P* velocity structure.

Our progress to date includes the development of some of the key components of our method. These include 1) surface-wave modeling algorithms to create phase and group velocity maps as a function of period; 2) enhancement of our tomography algorithm to derive either 3-D velocity models (for body-wave inversion) or 2-D group-velocity maps (for surface-wave inversion); and 3) improvements in the underlying inversion methodology to allow for velocity bounds and spatially variable smoothness constraints. In addition, we have generalized the interfaces between the various modules of our system to facilitate the integration of body-wave and surface-wave inversion results into a unified 3-D Earth model.

We will apply our joint inversion method to a large region covering central and southern Asia. The body-wave data consist of travel times derived from the Engdahl, van der Hilst and Buland (EHB) bulletin for the years 1988 – 2004. The surface-wave data consist of measured group velocities from the University of Colorado research team, as well as measurements from previous and ongoing experiments in the region of study.

OBJECTIVES

To improve earth structure and associated monitoring efforts, Weston Geophysical Corporation and the Earth Resources Laboratory at the Massachusetts Institute of Technology are collaborating to develop a joint 3-D inversion technique that incorporates both body-wave travel times and Rayleigh-wave group velocity measurements to determine the full *P* and *S* velocity structure of the crust and upper mantle. Research objectives include the following:

- Extension of our current inversion codes to produce improved 3-D estimates of the *P* structure from first-arrival body-wave travel times;
- Development of a sequential inversion technique to jointly invert both body-wave travel times and Rayleigh-wave group velocities for 3-D *P* and *S* velocity structure;
- Estimates of the *P* and *S* model uncertainty; and
- Validation of the new model using a variety of techniques, including location calibration and full-waveform modeling.

We will apply the new technique to data from the broad region shown in Figure 1. The unique and innovative contribution that will result from this project will be an inversion methodology that combines regional body and surface wave data to constrain Earth structure. The application of this methodology to construct and validate a regional *P* and *S* model for southern and central Asia may directly impact nuclear monitoring capabilities and provide useful information for other seismologists.

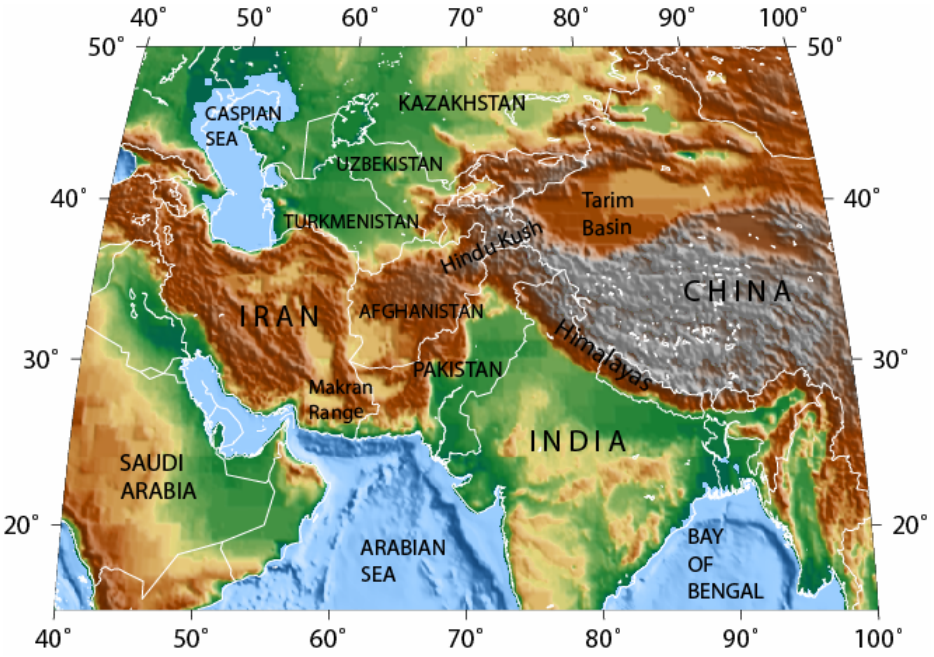

Figure 1. Map of study region.

RESEARCH ACCOMPLISHED

In the first year of the project we have focused on developing some of the core numerical techniques and software modules needed for our joint inversion approach. These have pertained mainly to the forward modeling method for surface-wave dispersion in 3-D Earth models, and the enhancements to the model parameterization and regularization employed in our underlying inversion algorithm. The next section describes our overall inversion approach and is followed by some specifics of the numerical techniques we have developed thus far.

Joint Inversion Approach

The starting point for this project was the regional travel-time tomography method developed by Reiter et al. (2005) and applied by them in India-Pakistan and by Murphy et al. (2005) in Russia and China. The method begins with a 3-D *P* velocity model for the crust and upper mantle, containing lateral variations both in velocity and in interface depths (e.g., the Moho). Forward modeling is performed with finite-difference ray tracing using the algorithm of Podvin and Lecomte (1991). The tomography method solves for an updated upper mantle *P* velocity based on *Pn* times observed from multiple earthquakes and stations in the model region. This earlier method restricts the velocity update in its parameterization by forcing built-in depth dependence. Essentially, the tomography solves for the velocity just below the Moho, and its difference from the initial model velocity at the same depth is extrapolated downward to a depth of 210 km and tapered linearly to zero between 210 km and 410 km. The free parameter in the inversion is thus a 2-D velocity function, latitude (θ) and longitude (φ).

This project is extending our original method by adding surface-wave dispersion data to the data set and the *S* velocity model to the inversion parameters. In addition, the velocity parameterization is more general, allowing full 3-D variation in the two unknown velocity functions: $v_P(\theta,\varphi,z)$ and $v_P(\theta,\varphi,z)$ (where z is depth).

For the time being, we are restricting the body-wave data to *Pn* travel times, and the surface-wave data to Rayleigh-wave group velocities at periods sensing upper mantle structure (periods greater than about 10 s). Accordingly, our method will initially solve for the 3-D velocity structure of the upper mantle between the Moho and the 410-km discontinuity, with the crustal velocities and crustal thickness held fixed to their initial (CRUST2.0) values. The techniques and software we are developing, however, will be sufficiently general to eventually accommodate additional data (e.g., *S* travel times, Love-wave dispersion, crustal body-wave phases, and a wider period band for dispersion) and additional model parameters (e.g., crustal velocities and Moho depth).

Given the initial focus of the project, one version of the methodology we are developing will perform body-wave and surface-wave inversion as separate procedures. That is, an inversion of *Pn* times will update v_P in the upper mantle and a separate inversion of Rayleigh-wave group velocities will update the upper mantle v_S (since the dependence of surface-wave dispersion on mantle *P* velocity is small). The two inversions will be coupled, however, through the prior information applied to the velocity functions. These will include smoothness constraints as well as prior upper and lower bounds on the velocity value at each point in the upper mantle. The bounds can be determined in part from bounds on Poisson's ratio, which would vary with depth and tectonic regime. In the surface-wave inversion, for example, bounds on v_S are implied by the current v_P model and the limits on Poisson's ratio. This will couple the body-wave and surface-wave inversions in a way that ensures consistency between the *P* and *S* velocity models. We plan to repeat the two inversions in an iterative process, which will solve the joint, nonlinear inverse problem.

Another key element of our approach is the factorization of the surface-wave inversion into two steps. In the first step, the group delays for the observed event-station pairs, for each frequency ω, are used to determine a group velocity map $u(\theta,\varphi,\omega)$. This inversion is effectively a 2-D tomography, performed frequency by frequency. The second step uses the resulting dispersion curve at each (θ,φ) to determine an *S* velocity-depth profile. This second step is a 1-D inversion performed separately for each latitude and longitude in the group velocity map, yielding collectively a 3-D velocity function $v_S(\theta,\varphi,z)$. This factorization was also done by Ritzwoller et al. (2002) and others and is compatible with the forward modeling method outlined in the next section.

The body-wave inversion will be a one-step, 3-D tomography that uses the observed *P* travel times over event-station paths to directly determine the 3-D velocity function $v_P(\theta,\varphi,z)$.

Forward Modeling of Surface-Wave Dispersion

Our approach for modeling surface wave dispersion in a 3-D Earth employs the same approximation used by Stevens and Adams (1999), Ritzwoller and Levshin (1998) and others, which states that the phase delay

($d^{ph}(\omega)$), or phase travel time, between an event and a station is obtained as an integral of the local phase velocity along a fixed travel path:

$$d^{ph}(\omega) = \int_{Path} \frac{ds}{c(\theta,\varphi,\omega)} . \qquad (1)$$

For each latitude/longitude point (θ,φ), $c(\theta,\varphi,\omega)$ is taken to be the dispersion response of the 1-D medium characterized by the velocity and density profiles at that point. For fixed frequency ω we refer to $c(\theta,\varphi,\omega)$ as a phase velocity *map*. Similarly, the *group* delay for the event-station pair is given by

$$d^{gr}(\omega) = \int_{Path} \frac{ds}{u(\theta,\varphi,\omega)} , \qquad (2)$$

where $u(\theta,\varphi,\omega)$ is the group velocity map. Typically the path integrations in Equations (1) and (2) are performed along the great circle connecting the source and receiver points (Woodhouse and Dziewonski, 1984). This is correct for a 1-D Earth model in which the local dispersion is the same at each latitude and longitude. However, lateral heterogeneities in the crust and upper mantle can cause both Rayleigh and Love waves to deviate laterally relative to the great-circle path. Many studies of regional and global surface wave propagation have observed off-great-circle path deviations. For example, Levshin et al. (1994) showed that regional structure in northern and central Eurasia caused significant departures from great-circle propagation, and recent studies by Cotte et al. (2000) demonstrated azimuthal deviations of up to 30° for surface waves between 20- and 40-second periods propagating in the French Alps.

A better approximation to phase and group travel times is found by integrating the phase and group slownesses along the minimum-time path through the frequency-specific, 2-D phase velocity map. Other researchers have used a paraxial, 2-D shooting, and finite-difference methods of raytracing to explore this approach (Ammon and Vidale, 1993; Bruneton et al., 2002; Kennett and Yoshizawa, 2002; Ritzwoller et al., 2002). We are using the Podvin-Lecomte ray-tracing technique (Podvin and Lecomte, 1991), as we do in body-wave modeling. In the body-wave application, we apply the Podvin-Lecomte (P-L) method to propagate first-arrival travel times from a given seismic station location through a 3-D medium to a 3-D grid of nodes, representing a grid of event hypocenters. The resulting 3-D travel-time grid can be interpolated to relevant event locations. Adapting the P-L ray tracer to 2-D dispersion modeling involves a multi-step process to obtain phase and group delays for various source-receiver paths. Here we illustrate these steps with our initial model, which consists of the CRUST2.0 3-D model (Bassin et al., 2000) tapered into the *iasp91* model (Kennett and Engdahl, 1991) at 210-km depth.

The first step of our modeling process is to compute the dispersion response for each geographic grid point of the 3-D Earth model, as determined by the 1-D velocity/density profile defined for each point. We perform these dispersion calculations using software adapted from a set of modal summation codes (Computer Programs in Seismology; Herrmann, 2002). Implicit in the use of these codes is an "Earth-flattening" transformation that corrects for the Earth's sphericity. We collate the output from these calculations at the frequencies of interest to produce a set of phase- and group-velocity maps, $c(x,y,\omega)$, and $u(x,y,\omega)$, respectively. Figure 2 shows the group-velocity maps (as percent deviation from the *iasp91* predicted group velocity) at periods of 10s, 15s, 20s, and 25s.

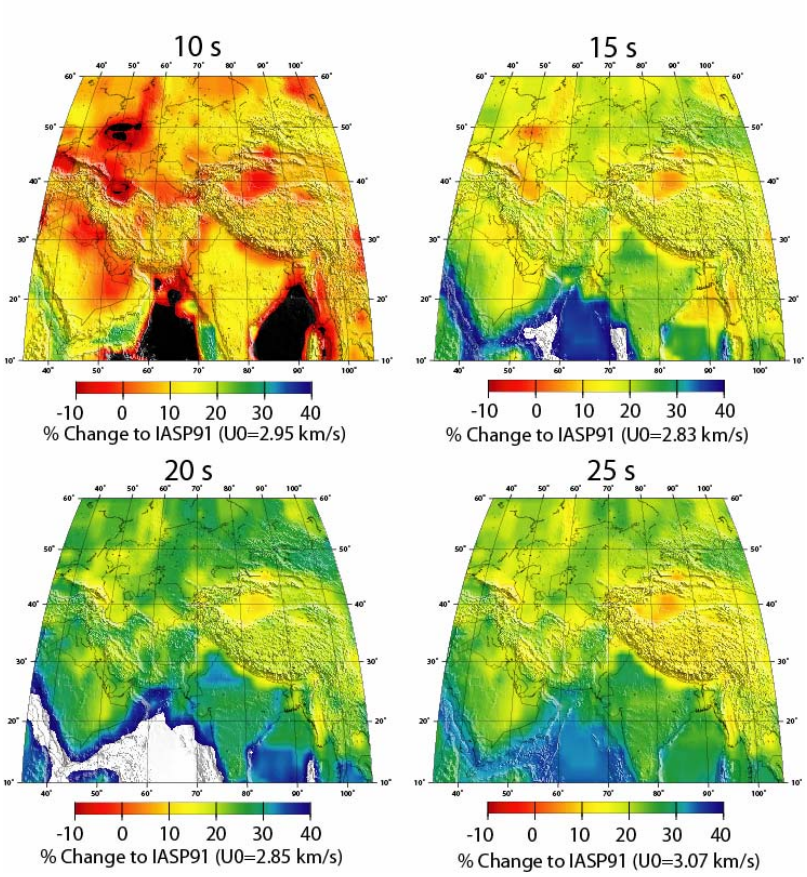

Figure 2. Initial model-predicted group velocities as a function of period, shown as a percent change from the constant (U0) velocity found using the 1-D *iasp91* model. The maps were generated using modal summation techniques at each nodal depth profile in the earth model.

The next step in the dispersion forward-modeling process is the calculation of phase-delay (or "phase-time") maps from the phase-velocity maps, using the P-L ray tracer. Our implementation of the P-L algorithm applies to flat Earth models represented by Cartesian grid of homogeneous velocity cells. Thus, on a station-by-station basis, we spatially interpolate each geographic phase velocity map onto a regular 2-D Cartesian grid based on a stenographic map projection. For example, Figure 3 shows the Cartesian phase-velocity maps that are generated from our initial model at periods of 10, 15, and 20 seconds for a 10-degree region around the station NIL (Nilore, Pakistan). In this example the Cartesian grid sampling was 10 km in x and y. (We are currently experimenting with the appropriate sampling interval to ensure travel-time prediction accuracy.) The regional variability of the velocity structure is clearly visible in the phase speed maps, where basins are delineated by low velocities and the Indian shield appears as a high in the southeastern corner of the maps. The strong low present in the southwest corner of the 10- and 15-second maps is the northeastern extreme of the Arabian Sea.

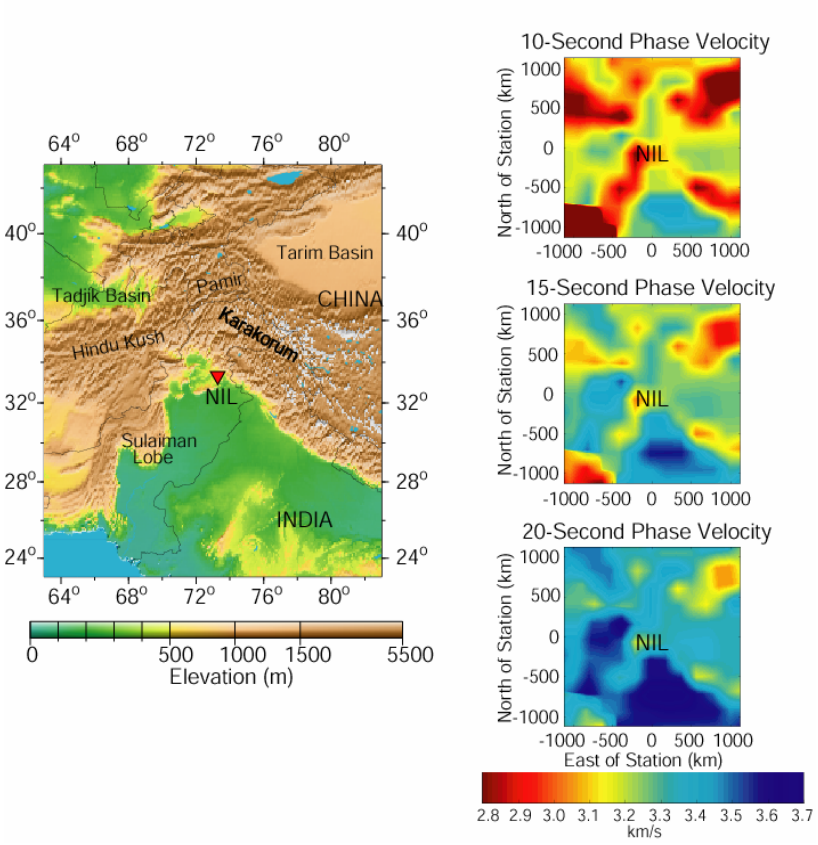

Figure 3. (Left) Topographic map of the NIL station and surrounding region out to 10° epicentral distance (Mercator projection). (Right) Cartesian maps of Rayleigh-wave phase velocities at 10-, 15-, and 20-seconds period based on our initial model. All phase-velocity maps are plotted on the same color scale.

For each station (and period), the 2-D version the P-L ray tracer creates a Cartesian grid of phase delays that represent the minimum travel time from the station location to each point in the Cartesian grid. The final step of our modeling process is to find the phase and group delays for the particular station/event pairs involved in the data set. For the phase delay, this is simply a matter of interpolating the calculated grid-point times to a particular event location (as transformed from geographic to Cartesian coordinates).

For the group delay, we must perform the integration indicated by Equation (2), where "*Path*" is taken to be the minimum phase-time ray path. In the P-L method, a ray path is represented by the sensitivities of the phase travel time to the phase velocities of cells, defined by

$$s_{lm}(\omega) = \frac{\partial d^{ph}(\omega)}{\partial c_{lm}^{-1}(\omega)}, \tag{3}$$

where ℓ and *m* index the cells of the 2-D Cartesian grid. The integral in Equation (2) is then approximated as

$$d^{gr}(\omega) = \sum_{\ell m} \frac{s_{\ell m}(\omega)}{u_{\ell m}(\omega)}. \tag{4}$$

We compute the cell sensitivities, $s_{\ell m}$, using an extension to the P-L code we used in our previous work (Reiter et al., 2005) to calculate sensitivities for body-wave travel times. The sensitivities of travel times to

cell slownesses are computed using recursive back-propagation of node-to-node and node-to-cell dependencies from any given receiver point (event position) toward the source (station position). Consistent with the underlying ray theory, the resulting sensitivities are concentrated along a trajectory of cells connecting the source and receiver points, and this trajectory defines the P-L version of a ray path.

In Figure 4 we depict the path sensitivities that are derived from the 20-second Rayleigh phase-speed map for a set of four events in the region surrounding NIL. The figure shows that out-of-plane (or non-great-circle path) propagation is present at the 20-second period for our 3-D initial model.

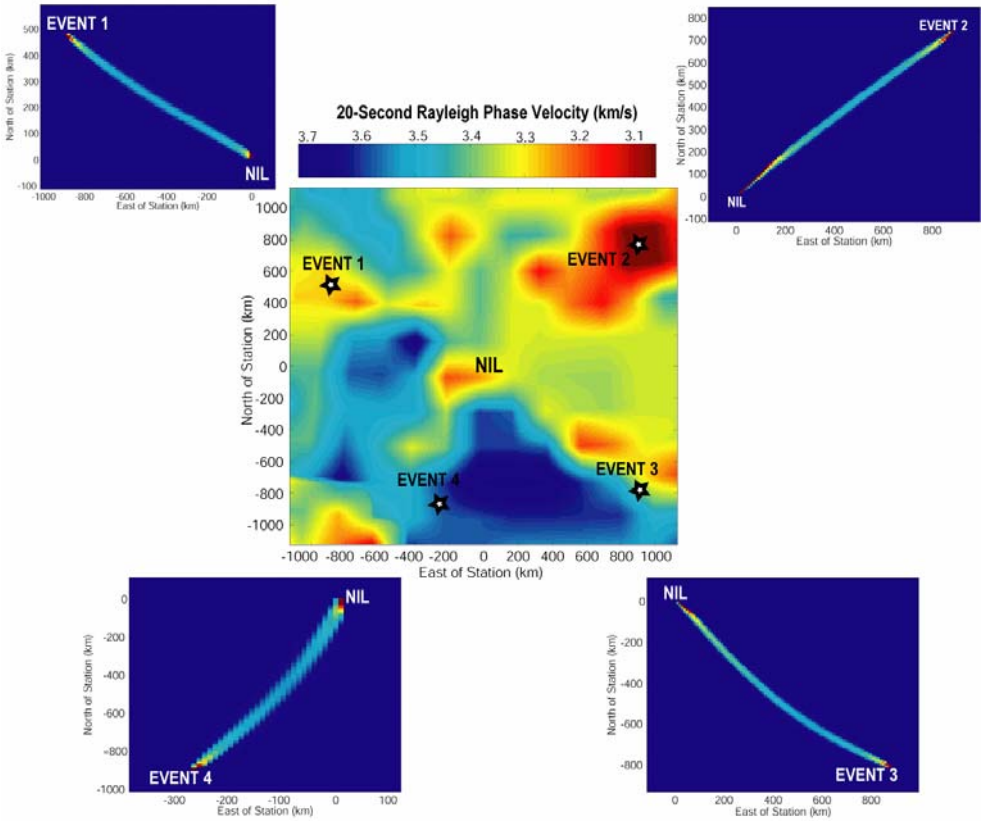

Figure 4. (Middle subplot) Phase velocity map at a period of 20 seconds surrounding station NIL. Plotted around the velocity map are four event positions, for which ray sensitivities have been calculated (each ray subplot is labeled according to its respective event). Note that the rays do not travel along great-circle paths.

Sensitivities are also needed to perform tomographic inversion, i.e., fitting group velocity maps to the group delays observed over particular paths. To create these, the $s_{\ell m}(\omega)$, defined on the P-L Cartesian grid, are transformed to sensitivities to the nodal values of the group velocity maps in geographic coordinates ($u(\theta,\varphi,\omega)$) using the inverse of the interpolation transformation that generated the Cartesian cell velocities.

Inversion Method

The inversion method used by Reiter et al. (2005) to estimate the *Pn* lid-velocity map, $v_{lid}(\theta,\varphi)$, was a regularized least squares technique. The inversion model function was taken to be the *Pn*-lid slowness:

$$m(\theta,\varphi) = \frac{1}{v_{lid}(\theta,\varphi)}, \tag{5}$$

and the solution to the inverse problem was defined as the function *m* that minimizes the objective function given by

$$\Psi = \sum_{ij} \left| d_{ij} - F_{ij}(m) \right|^2 / \sigma_{ij}^2 + \lambda\, S(m). \tag{6}$$

In the first term, d_{ij} is the observed travel-time datum for the i^{th} event and j^{th} station; σ_{ij} is the standard deviation of the observational error in the datum; and F_{ij} is the forward modeling function for the datum (F_{ij} computes the Podvin-Lecomte travel time through the 3-D model extrapolated from v_{lid}). In the second term, *S(m)* is a stabilizing function which we set to

$$S(m) = \iint (\nabla^2 m)^2 \, d\theta \, d\varphi. \tag{7}$$

This term serves to constrain the spatial roughness of *m*, with the regularization parameter, λ, controlling the strength of the constraint. We performed the minimization of Ψ by iterating over the linearized problem, in which each F_{ij} is replaced by its first-order expansion with respect to the current solution, as expressed with the sensitivities of F_{ij} to the nodal values of *m* that parameterize the model function.

In this project we are developing significant extensions of this inversion method. Here we describe three that we are implementing in the body-wave inversion step of our joint tomography method. First, the 2-D model function is being replaced with a 3-D function that provides explicitly for lateral and vertical *P* velocity variations in the upper mantle. Denoting the *P* velocity simply as *v*, the model function becomes

$$m(\theta, \varphi, z) = \frac{1}{v(\theta, \varphi, z)}, \tag{8}$$

where *z* ranges between the Moho and the 410-km discontinuity. This replacement is facilitated by the fact that our earlier method derived the 2-D travel-time sensitivities to $1/v_{lid}$ from the 3-D slowness sensitivities, which are now used directly.

Second, our new method will apply hard bounds to the velocity function as a constraint on the minimization of Ψ. This is being done as follows: let the bounds be expressed as

$$v_-(x) \le v(x) \le v_+(x), \tag{9}$$

where we let $x = (\theta,\varphi,z)$ for conciseness. We can satisfy this automatically with an appropriate transformation of the model function *m* to velocity. The transformation we are using at this time employs the error function (*erf*):

$$\frac{1}{v(x)} = \frac{1}{2}\left[\frac{1}{v_-(x)} + \frac{1}{v_+(x)}\right] + \frac{1}{2}\left[\frac{1}{v_-(x)} - \frac{1}{v_+(x)}\right] erf(\beta(x) m(x)), \tag{10}$$

where $\beta(x)$ is a specified scaling parameter. Since the error function traverses -1 to 1 as *m* ranges from $-\infty$ to ∞, Equation (9) is obeyed without constraining *m* in the minimization of Ψ. A disadvantage of this technique is that the forward modeling functions, $F_{ij}(m)$, become nonlinear even for linearized (fixed ray) tomography. We are addressing this by using a *nonlinear* conjugate gradients technique to minimize Ψ.

The third extension of the tomography method we are in the process of implementing is the replacement of the stabilizing function with a more general form that is motivated by geostatistical concepts, as are used in kriging (e.g., Deutsch and Journel, 1998). The mathematical development of the new stabilizing function is described by Rodi et al. (2005) and Murphy et al. (2005). The functional form is given by

$$S(m) = \int m(x)\big[Dm\big](x)\, dx, \tag{11}$$

where *D* is a specified differential operator. Our earlier method (Equation (7) took *D* to be the biharmonic (squared Laplacian) operator. An example of a geostatistically based *D* is

$$D = \frac{1}{8\pi\lambda^2\sigma_0^2}\left[\delta(x) - \lambda^2\nabla^2\right]^2 . \qquad (12)$$

This operator treats *m(x)* as a stationary Gaussian random field with variance σ_0^2, correlation length λ, and a spatial correlation function of the exponential type (see Deutsch and Journel, 1998). We have implemented this and the larger class of differential operators considered by Rodi et al. (2005) using difference operators in spherical coordinates, consistent with the geographic model parameterization used in our tomography method. We are extending these operators to allow the geostatistical parameters (e.g., σ_0) to vary spatially, which provides a mechanism for varying the smoothness constraints in accordance with the ray coverage of the data set.

Joint Tomography Data Set

We will apply our joint inversion algorithm to a large database of first-arriving *P* and *S* travel times and fundamental-mode phase and group velocity measurements. Most of our data come from public sources, but we will also be incorporating travel-time and group velocity measurements from Weston's ongoing regional experiments.

The body-wave data set is composed of origin parameters and associated arrival times for a set of well-located seismic sources from the Engdahl et al. (1998; EHB) bulletin. We use several filtering criteria to limit the occurrence of residuals not related to velocity variations. These criteria include limitations on event depths, epicentral distances, and magnitudes. Distance and depth ranges are chosen to isolate waves propagating in the crust and upper mantle from faster, deeper traveling *P* waves. To ensure that an event's epicentral mislocation is no worse than 15 km for 85% of the events, we require the secondary azimuth gap (defined as the largest azimuthal gap filled by a single station) for a given event to be less than or equal to 130º (Bondár et al., 2004). To minimize the inherent picking error, we require the *P*-phase arrival times to be designated as impulsive and restrict the travel-time residuals with respect to the *iasp91* model to less than ±7 seconds.

The surface-wave database consists of phase- and group-velocity dispersion measurements from paths sampling our region of interest. We received our initial data set from the group at the University of Colorado at Boulder (Ritzwoller and Levshin, 1998). It comprises over 97,000 group velocity measurements at periods between 10 – 250 seconds. This database is especially rich in the short-period measurements that will constrain the crust and upper mantle portion of our model.

CONCLUSIONS AND RECOMMENDATIONS

Our first year's effort on this project has produced the overall design of the methodology we will use to perform joint body-wave and surface-wave regional tomography, which we are implementing in a set of integrated software modules for constructing calibrated 3-D Earth models and performing event location based on these models. Our initial focus on 3-D upper mantle *P* and *S* velocity structure in south/central Asia, inferred from *Pn* travel times and intermediate-period Rayleigh wave group velocities, is the natural extension of our earlier work on *Pn* tomography in India and Pakistan. The ultimate goal of the project, however, is to create a general capability for constructing full 3-D crust and upper mantle models for areas of monitoring interest around the world based on the available body-wave and surface-wave observations, including *P* and *S* travel times observed at local and regional distances, and regional Rayleigh and Love wave dispersion observed over a broad frequency band.

ACKNOWLEDGEMENTS

We are grateful to Dr. Bob Engdahl for providing updated versions of his event bulletin. We sincerely appreciate the extensive dispersion measurements provided by Prof. Mike Ritzwoller's group at the

University of Colorado. All maps were produced using the Generic Mapping Tools (GMT) data processing and display package (Wessell and Smith, 1991; 1995).

REFERENCES

Ammon, C. J. and J. E. Vidale (1993), Tomography without rays, *Bull. Seism. Soc. Amer*. 83: 509–528.

Bassin, C., G. Laske and G. Masters (2000), The Current Limits of Resolution for Surface Wave Tomography in North America, *EOS Trans AGU* 81: F897.

Bondár, I., E. R. Engdahl, X. Yang, H. A. A. Ghalib, A. Hofstetter, V. Kirichenko, R. Wagner, I. Gupta, G. Ekström, E. Bergman, H. Israelsson and K. McLaughlin (2004). Collection of a reference event set for regional and teleseismic location calibration, *Bull. Seism. Soc. Amer.* 94 1528–1545.

Bruneton, M., V. Farra, H. A. Pedersen and the SVEKALAPKO Seismic Tomography Working Group (2002), Non-linear surface wave phase velocity inversion based on ray theory, *Geophys. J. Int*. 151: 583–596.

Cotte, N., H. A. Pedersen, M. Campillo, V. Farra and Y. Cansi (2000), Off-great-circle propagation of intermediate-period surface waves observed on a dense array in the French Alps, *Geophys. J. Int*. 142: 825–840.

Deutsch, C. V. and A. G. Journel (1998), GSLIB: *Geostatistical Software Library and User's Guide*, 2nd ed., Oxford University Press, Inc., New York, 369 pp.

Engdahl E. R., R. van der Hilst, and R. Buland (1998), Global teleseismic earthquake relocation with improved travel times and procedures for depth determination, *Bull. Seism. Soc. Amer*. 88: 722–743.

Herrmann, R. B. (2002), *Computer Programs in Seismology*, Version 3.20, St. Louis University.

Kennett, B. L. N. and E. R. Engdahl (1991), Travel times for global earthquake location and phase identification*, Geophys. J. Int*. 105 429–465.

Kennett, B. L. N. and K. Yoshizawa (2002), A reappraisal of regional surface wave tomography, *Geophys. J. Int*. 150: 37–44.

Levshin, A. L., M. H. Ritzwoller, and L. I. Ratnikova (1994), The nature and cause of polarization anomalies of surface waves crossing northern and central Eurasia, *Geophys. J. Int*. 117: 577–590.

Murphy, J. R., W. Rodi, M. Johnson, D. D. Sultanox, T. J. Bennett, M. N. Toksöz, V. Ovtchinnikov, B. W. Barker, D. T. Reiter, A. M. Rosca, and Y. Shchukin (2005), Calibration of International Monitoring System (IMS) stations in central and eastern Asia for improved seismic event location, *Bull. Seism. Soc. Amer.* 95: 4.

Podvin, P., and I. Lecomte (1991), Finite difference computation of travel times in very contrasted velocity models: a massively parallel approach and its associated tools, *Geophys. J. Int.* 105: 271–284.

Reiter, D., W. Rodi, and M. Johnson (2005), Development of a tomographic upper-mantle velocity model beneath Pakistan and northern India for improved regional seismic event location, 95, 926–940.

Ritzwoller, M. H., and A. L. Levshin (1998), Eurasian surface wave tomography: Group velocities, *J. Geophys. Res.,* 103, B3, 4839–4878.

Ritzwoller, M. H., N. M. Shapiro, M. P. Barmin and A. L. Levshin (2002), Global surface wave diffraction tomography, *J. Geophys. Res*. 107**:** doi: 10.1029/2002JB001777.

Rodi, W., C. A. Schultz, G. Johannessen, and S. C. Myers (2005), Grid-search location methods for ground-truth collection from local and regional seismic networks, Final Technical Report to National Nuclear Security Administration, Dept. of Energy, Contract Nos. DE-FC03-01SF22397 and W-7405-ENG-48.

Stevens, J. L. and D. A. Adams (1999), Improved surface wave detection and measurement using phase-matched filtering and improved regionalized models, in *Proceedings of the 21st Seismic Research Symposium*, *Technologies for Monitoring the Comprehensive Nuclear-Test-Ban-Treaty,* Los Alamos National Laboratory document LA-UR-99-4700, Las Vegas, NV, 274–282.

Wessel, P. and W. H. F. Smith (1991). Free software helps map and display data, *Eos Trans. AGU* 72: 441, 445–446.

Wessel, P. and W. H. F. Smith (1995). New version of the Generic Mapping Tools released, *Eos Trans. AGU* 76: 329.

Woodhouse, J. H. and A. M. Dziewonski (1984), Mapping the upper mantle: three-dimensional modeling of Earth structure by inversion of seismic waveforms, *J. Geophys. Res*. 89: 5953–5986.